Weaving Knotted Vector Fields with Tunable Helicity

Hridesh Kedia,[1,*] David Foster,[2] Mark R. Dennis,[2] and William T. M. Irvine[1]
[1]Department of Physics, James Franck Institute, Enrico Fermi Institute, The University of Chicago, 929 E 57th St., Chicago, Illinois 60637, USA
[2]HH Wills Physics Laboratory, University of Bristol, Tyndall Avenue, Bristol BS8 1TL, UK
(Received 17 July 2016; published 29 December 2016)

We present a general construction of divergence-free knotted vector fields from complex scalar fields, whose closed field lines encode many kinds of knots and links, including torus knots, their cables, the figure-8 knot, and its generalizations. As finite-energy physical fields, they represent initial states for fields such as the magnetic field in a plasma, or the vorticity field in a fluid. We give a systematic procedure for calculating the vector potential, starting from complex scalar functions with knotted zero filaments, thus enabling an explicit computation of the helicity of these knotted fields. The construction can be used to generate isolated knotted flux tubes, filled by knots encoded in the lines of the vector field. Lastly, we give examples of manifestly knotted vector fields with vanishing helicity. Our results provide building blocks for analytical models and simulations alike.

DOI: 10.1103/PhysRevLett.117.274501

Introduction.—The idea that a physical field—such as a magnetic field—could be weaved into a knotty texture has fascinated scientists ever since Lord Kelvin conjectured that atoms were, in fact, vortex knots in the aether. Since then, topology has emerged as a key organizing principle in physics, and knottiness is being explored as a fundamental aspect of classical and quantum fluids [1–8], magnetic fields in light and plasmas [9–19], liquid crystals [20–23], optical fields [24,25], nonlinear field theories [26–29], wave chaos [30], and superconductors [31,32].

In particular, helicity—a measure of average linking of field lines—is a conserved quantity in ideal fluids [33,34] and plasmas [35–37]. Helicity thus places a fundamental topological constraint on their evolution [1,10], and plays an important role in turbulent dynamo theory [38–40], magnetic relaxation in plasmas [41–43], and turbulence [44,45]. Beyond fluids and plasmas, helicity conservation leads to a natural connection between the minimum energy configurations of knotted magnetic flux tubes [10,42,46] and tight knot configurations [47,48], and tentatively with the spectrum of mass energies of glueballs in the quark-gluon plasma [49–51].

Knotted field configurations provide a natural setting for studying helicity, but more subtlety is required to tie a knot in the lines of a vector field than in a shoelace: all the streamlines of the entire space-filling field must twist to conform to the knotted region. The difficulty of constructing knotted field configurations with controlled helicity makes it challenging to understand the role of helicity in the evolution of knotted structures [1,10,12].

In this Letter, we show how to explicitly construct knotted, divergence-free vector fields with a wide range of topologies, which have finite energy and tunable helicity and give a systematic prescription for calculating the helicity of these knotted fields.

Studying the dynamics of these knotted field configurations in fluids and plasmas may deepen our understanding of helicity, give insights into the longstanding problem of "magnetic relaxation under topological constraints" [52], and help understand the stability of plasmas in knotatrons —magnetic confinement devices in the shape of knots [53].

A classical problem from mathematics is the study of knots and links as nodal lines (zeros) of complex scalar fields [25,54–57]. In fact, the level sets of a complex scalar field can give rise to collections of knotted curves that smoothly intertwine to fill up space. Well-known examples are the Hopf fibration [11,13,14,58–60], Seifert fibrations [15,61] and Milnor fibrations [25,54,62]. Many knots can be embedded as the nodal lines of complex scalar fields in the family of lemniscate knots and their generalizations [63], which includes all torus knots and links [55], the figure-8 knot and generalizations [25] (including the Borromean rings), cable knots [64], and links of any of these.

Some representative examples of knotted complex scalar fields are illustrated in Fig. 1, where the level curves wind around knotted or linked tori, encoding the Hopf link [Fig. 1(b)], the trefoil knot [Fig. 1(c)], the figure-8 knot [25] [Figs. 1(a) and 1(d)], a link of two trefoils [Fig. 1(e)], and a cable knot [Fig. 1(f)]. In all of these examples, the level curves of the complex scalar field ψ, for any complex value of ψ, organize around a core set of lines where $\psi = 0, \infty$ (zeros and poles of ψ). Our construction of knotted vector fields follows from such knotted complex scalar fields, based on [29,55,63], where the level curves of constant complex amplitude are collections of knotted curves filling up space.

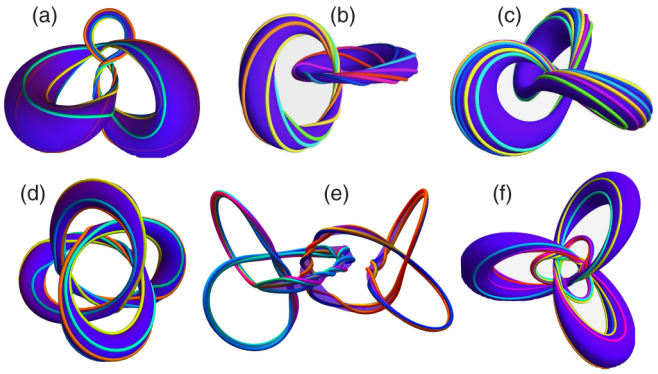

FIG. 1. Knotted structures encoded in the level sets of the complex scalar fields $\psi = P(u,u^*,v,v^*)/Q(u,u^*,v,v^*)$, where (u,v) are functions of (x,y,z) [see Eq. (3)]. (a) Figure-8 knots: $\psi = v/[64u^3 - 12u(3-2v^2+2v^{*2}) + (14v^2+14v^{*2}-v^4+v^{*4})]$. (b) Linked rings: $\psi = u^2/(u^2-v^2)$. (c) Trefoil knots: $\psi = u^3/(u^3+v^2)$. Level curves of ψ encode torus knots and links when $Q(u,v)$ is of Brieskorn form [54]: $u^p + v^q$. (d) Figure-8 knots (symmetric): $\psi = u/[64v^3 - 12v(3+2u^2-2u^{*2}) - (14u^2+14u^{*2}+u^4-u^{*4})]$. (e) Linked trefoil knots, constructed from 2 copies of the Milnor polynomial for a trefoil knot. See Supplemental Material [65] for details. (f) $C^{2,3}_{3,2}$ cable knots: $\psi = (uv)/(v^4 - 2u^3v^2 - 2iu^3v + u^6 + \frac{1}{4}u^3)$.

A vector field tangent to the level curves of a complex scalar field ψ is given simply by the cross product $-i\nabla\psi^* \times \nabla\psi = \nabla \times \mathrm{Im}(\psi^*\nabla\psi)$. A vector field with the same flow lines is

$$\mathbf{B} = \frac{1}{2\pi i}\frac{\nabla\psi^* \times \nabla\psi}{(1+\psi\psi^*)^2}. \tag{1}$$

This field is smooth everywhere, divergence free ($\nabla\cdot\mathbf{B} = 0$), and has finite energy ($\int d^3x|\mathbf{B}|^2 < \infty$). This vector field arises in a variety of different contexts, and was used previously to construct knotted initial states for electromagnetic fields [11,15] and topological solitons in ideal magnetohydrodynamics [9].

Since the flow lines of $\mathbf{B}$ (i.e., the level sets of ψ) can clearly be knotted, it is natural to suppose that such fields have nontrivial helicity. Explicitly calculating the helicity $\mathcal{H} = \int d^3x\mathbf{A}\cdot\mathbf{B}$ requires the choice of a vector potential $\mathbf{A}$ such that $\nabla\times\mathbf{A} = \mathbf{B}$. A natural candidate,

$$\mathbf{A} = \frac{1}{4\pi i}\frac{(\psi^*\nabla\psi - \psi\nabla\psi^*)}{(1+\psi^*\psi)}, \tag{2}$$

suggests that the helicity of the knotted vector field $\mathbf{B}$ vanishes. We will show that $\mathbf{A}$ in Eq. (2) has a singular part which can be systematically removed, leading to a nonsingular vector potential, which allows explicit calculation of the helicity of all these knotted fields.

The helicity of the resulting knotted vector field can be computed explicitly, and may be varied without changing the underlying knotted structure. Furthermore, these fields may be restricted to the interior of knotted flux tubes [66] whose helicity can be calculated exactly. Lastly, we construct knotted fields with vanishing total helicity, but nonvanishing helicity in the interior of knotted flux tubes—tori tangent to the lines of $\mathbf{B}$.

Rational maps.—Rational maps have found success in approximating certain minimum energy solutions of the Skyrme model [68], and this technique was extended by Sutcliffe [29] to approximate knotted solutions of the Skyrme-Faddeev model. The knotted vector field construction described here is based on rational maps of similar form. A rational map is defined as the ratio of two complex-valued polynomials $\psi = P(u,u^*,v,v^*)/Q(u,u^*,v,v^*)$, where the nodal lines (zeros) of $Q(u,u^*,v,v^*)$ have the form of the desired knot, and $P(u,u^*,v,v^*)$ is chosen to encode the desired helicity [Fig. 4]. Here, as in Fig. 1, (u,v) are complex coordinates on S^3, which stereographically project (see Supplemental Material [65]) to coordinates (x,y,z) in $\mathbb{R}^3$ by

$$u = \frac{2(x+iy)}{1+r^2}, \qquad v = \frac{2z+i(r^2-1)}{1+r^2}, \tag{3}$$

where $r^2 = x^2+y^2+z^2$, and (u^*,v^*) denote complex conjugates of (u,v).

Such ψ automatically give rise to a vector field $\mathbf{B}$ as in Eq. (1), whose flow lines coincide with the level curves of ψ. The core set of lines that organize the flow lines of $\mathbf{B}$ are the zeros of P and Q (see Fig. 2). A wide variety of knotted

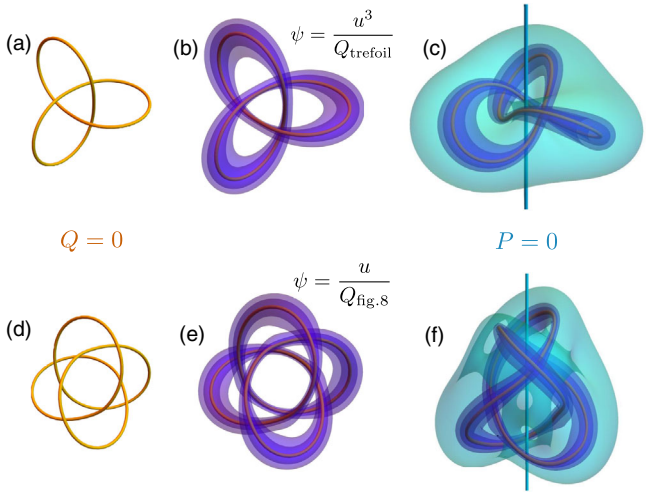

FIG. 2. Organization of the lines of $\mathbf{B}$ around lines where $\psi = P(u,v)/Q(u,v)$ is 0 or ∞. (a), (d) $Q = 0$ corresponds to the trefoil and figure-8 knots. $Q_{\text{trefoil}} = u^3+v^2$, $Q_{\text{fig-8}} = 64v^3 - 12v(3+2u^2-2u^{*2}) - (14u^2+14u^{*2}+u^4-u^{*4})$. (b), (e) The lines of $\mathbf{B}$ are tangent to nested knotted tori (blue), organized around the knots where $Q = 0$. (c),(f) $P(u,v) = 0$ corresponds to the z axis. The lines of $\mathbf{B}$ are tangent to nested tori (cyan) organized around $P(u,v) = 0$.

fields $\mathbf{B}$ can be constructed from rational maps ψ by encoding the desired knot in the zeros of $Q(u,u^*,v,v^*)$ for the various kinds of knot listed above (see Supplemental Material [65] for details).

Structure of knotted field lines.—We rewrite $\mathbf{B}$ using Euler potentials [69–72]:

$$\mathbf{B} = \nabla\left(\frac{\psi\psi^*}{1+\psi\psi^*}\right)\times\frac{1}{4\pi i}\nabla\log\left(\frac{\psi}{\psi^*}\right) = \frac{1}{2\pi}\nabla\chi\times\nabla\eta, \tag{4}$$

where $\chi = (\psi\psi^*)/(1+\psi\psi^*)$, $\chi\in[0,1]$, and $\eta = (1/2i)\log(\psi/\psi^*)$, $\eta\in[0,2\pi)$. We note that as $r\to\infty$, $|\nabla\chi|\sim O(1/r)$, $|\nabla\eta|\sim O(1/r)$, so that the energy density $|\mathbf{B}|^2\sim O(1/r^4)$ and the energy of all such fields, as the square integral of $\mathbf{B}$, is finite.

The lines of $\mathbf{B}$ are tangent to surfaces of constant χ and Seifert surfaces of constant η (see Fig. 3), which can be considered as a generalization of the surfaces of constant $\rho(\leftrightarrow\chi)$ and constant $\phi(\leftrightarrow\eta)$ in cylindrical coordinates (ρ,ϕ,z), with the knot $Q=0$ replacing the z axis.

The surfaces of constant χ are knotted tori, nested inside one another (Fig. 3), with smaller values of χ corresponding to larger tori, and the largest value $\chi=1$ corresponding to the knot $Q=0$ at the center of the tori [Figs. 2(a) and 2(d)]. Isosurfaces of smaller χ are increasingly bigger knotted tori, eventually colliding to give tori organized around $P=0$, as shown in Figs. 2(c) and 2(f) in cyan, which converge to the lines $P=0$ as $\chi\to 0$.

By contrast, η is constant on Seifert surfaces for the core set of lines: $P=0$, $Q=0$. Seifert surfaces for $Q=0$ are shown in Fig. 3. Since η is well defined only in a multiply connected volume, which excludes the core set of lines, the helicity of $\mathbf{B}$ can be nonvanishing [73], in spite of being expressible in terms of Euler potentials.

Helicity calculation.—A smooth vector potential $\mathbf{A}$ satisfying $\nabla\times\mathbf{A}=\mathbf{B}$ is needed to calculate the helicity $\mathcal{H}=\int d^3x\mathbf{A}\cdot\mathbf{B}$ of these knotted fields explicitly. We now give a general prescription for computing such a vector potential, starting by rewriting $\mathbf{A}$ in Eq. (2) as

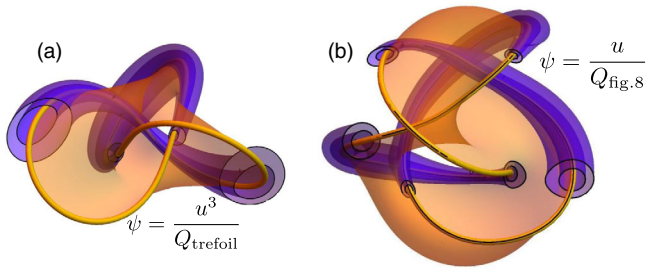

FIG. 3. Knotted field structures: knotted flux surfaces (blue) are surfaces of constant χ, and Seifert surfaces for $Q(u,u^*,v,v^*)=0$ (orange) are surfaces of constant $\log(Q/Q^*)$. (a) Trefoil knot with Q_{trefoil}, (b) Figure-8 knot with $Q_{\text{fig-8}}$ are defined in Fig. 2.

$$\mathbf{A} = \frac{1}{4\pi i}\left(\frac{\psi\psi^*}{1+\psi\psi^*}\right)\nabla\log\left(\frac{\psi}{\psi^*}\right). \tag{5}$$

Substituting $\psi = P(u,u^*,v,v^*)/Q(u,u^*,v,v^*)$ gives

$$\mathbf{A} = \frac{1}{4\pi i}\times\left[\frac{|P|^2\nabla\log(\frac{P}{P^*})+|Q|^2\nabla\log(\frac{Q}{Q^*})}{|P|^2+|Q|^2} - \nabla\log\left(\frac{Q}{Q^*}\right)\right] \tag{6}$$

The last term containing $\nabla\log(Q/Q^*)$ is singular at $Q=0$. Since $|Q|^2\nabla\log(Q/Q^*) = Q^*\nabla Q - Q\nabla Q^*$, this term in the fraction is smooth and nonsingular.

Hence, the singular gauge transformation $\tilde{\mathbf{A}} = \mathbf{A} + (1/4\pi i)\nabla\log(Q/Q^*)$ removes the singularity in $\mathbf{A}$, allowing the helicity to be computed directly. The vector potential $\tilde{\mathbf{A}}$ is smooth everywhere, giving the correct helicity $\mathcal{H}=\int d^3x\tilde{\mathbf{A}}\cdot\mathbf{B}$, which is equal to the Hopf invariant of the map ψ [29,74] by the Whitehead integral formula. Hence, we can explicitly compute the helicity [75] of arbitrary knotted fields $\mathbf{B}$ and therefore, the Hopf invariant of arbitrary rational maps.

Surfaces of constant $\log(Q/Q^*)$ yield explicit expressions for Seifert surfaces of the knot $Q(u,u^*,v,v^*)=0$ (see Fig. 3) and could be used to generate initial wave functions describing knotted vortices in superfluids and Bose-Einstein condensates.

The simplest illustration of our construction is given by the Hopf map [11,13,58–60] $\psi = u/v$. The vector potential given by Eq. (5) has a singularity at $v=0$ (the unit circle in the xy plane), which is removed via the singular gauge transformation $\tilde{\mathbf{A}} = \mathbf{A} + (1/4\pi i)\nabla\log(v/v^*)$. The new vector potential $\tilde{\mathbf{A}}$ is smooth everywhere and gives the correct helicity $\mathcal{H}=\int d^3x\tilde{\mathbf{A}}\cdot\mathbf{B}=1$, equal to the Hopf invariant of the map [29,74].

Tuning the helicity of a knotted field.—The helicity of $\mathbf{B}$ can be tuned without changing the underlying knotted structure encoded in $\mathbf{B}$, as for rational maps [29]. The flow lines of $\mathbf{B}$, contained in the knotted tori of constant χ in the neighborhood of the knot $Q=0\Leftrightarrow\chi=1$, encode knots of the same type as the knot $Q=0$. However, the degree of winding of these lines—and hence the helicity of $\mathbf{B}$—can be controlled by changing $P(u,v)$, as illustrated in Fig. 4.

Knotted fields encoding torus knots and links can be constructed from maps $\psi = P(u,v)/Q(u,v)$, with $P(u,v)=u^\alpha v^\beta$, $Q(u,v)=u^q+v^p$. The helicity of these fields can be varied without changing the underlying knotted structure by changing α, β in $P(u,v)=u^\alpha v^\beta$. The helicity of $\mathbf{B}$, being equal to the Hopf invariant [29,74] of the map ψ, is $\mathcal{H}=\alpha p+\beta q$. The lines of the field $\mathbf{B}$ wind more for higher values of α, β, as indicated by the higher values of helicity.

Knotted fields encoding other knot types such as lemniscate knots, cable knots, and iterated torus links can be constructed from maps $\psi = u^\alpha/Q(u,u^*,v)$

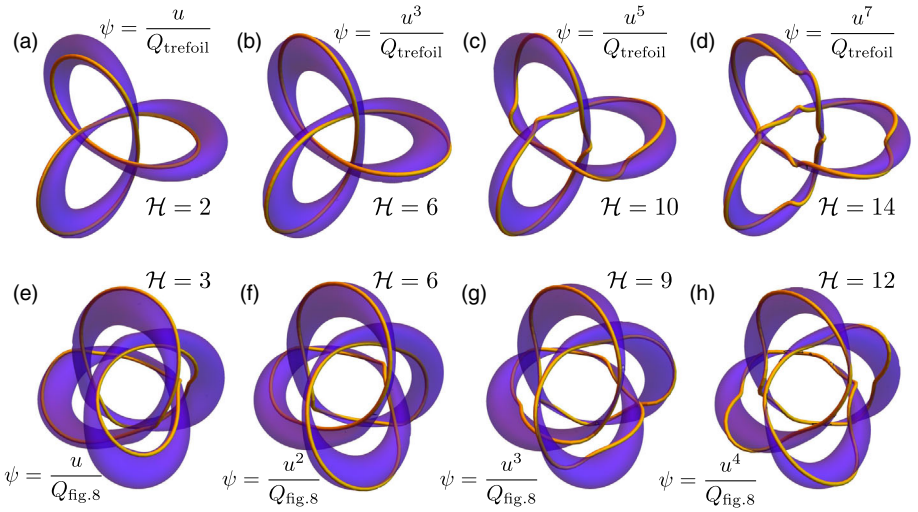

FIG. 4. Tuning the helicity $\mathcal{H}$ of the knotted field $\mathbf{B}$ by changing P for two fixed knot types (set by $\leftrightarrow Q$). Varying the helicity corresponds to varying amounts of winding of the lines of $\mathbf{B}$. (a)–(d): Trefoil knots with Q_{trefoil}, (e)–(h): Figure-8 knots with $Q_{\text{fig}-8}$, with Q functions as defined in Fig. 2.

[25,63,64,76]. Their helicity is given by $\mathcal{H} = \alpha \deg_v(Q)$, where $\deg_v(Q)$ is the highest power of v appearing in $Q(u, u^*, v)$ and can be tuned by changing α.

The helicity of such knotted fields $\mathbf{B}$ can be tuned further to yield negative values by substituting P or Q with their complex conjugates.

Helicity of knotted flux tubes.—Knotted flux tubes, magnetic flux tubes in plasmas, or vortex tubes in fluid can be generated by restricting the knotted field $\mathbf{B}$ to the interior of a knotted tube (Fig. 3): $\chi > \chi_0$ (see Supplemental Material [65]). Such a knotted flux tube contains flux $(1 - \chi_0)$, and its helicity can be calculated as in [12,67] to be $\mathcal{H}_{\chi_0} = (1 - \chi_0)^2 \mathcal{H}_{\text{total}}$, as the helicity for a uniformly twisted field with twist equal to $\mathcal{H}_{\text{total}}$.

Knotted fields with vanishing helicity.—Knotted fields $\mathbf{B}$, constructed from rational maps $\psi = P$ (i.e., $Q = 1$), have vanishing helicity, despite having knotted field lines.

This because vector potential $\mathbf{A}$ in Eq. (2) is singularity free, implying $\mathcal{H} = 0$. Geometrically, the lines of $\mathbf{B}$ tangent to the different knotted tori are of different handedness, and the average linking between the lines vanishes. However, the lines of $\mathbf{B}$ in the interior of a knotted torus—such that the lines of $\mathbf{B}$ are tangent to the torus, i.e.. the torus is a magnetic surface, so that the helicity in the torus is gauge invariant—may have nonvanishing helicity, which is difficult to compute analytically (see Supplemental Material [65]).

Alternatively, the vanishing of total helicity follows from the vanishing of the Hopf invariant [29,74] of the map given by $\psi = P(u, u^*, v, v^*)$, since the set of (u, u^*, v, v^*), such that $\psi = \infty$ is a null set.

Summary.—We have presented a general method for constructing physically viable knotted vector fields, encoding an arbitrary combination of knots woven together and shown how to explicitly compute their helicity. Furthermore, we have shown how to construct knotted flux tubes, and calculate their helicity.

Knotted fields arising as solutions to Maxwell's equations [19] have found application in the construction of topological solitons in magnetohydrodynamics [16] and resistive MHD flows [17]. The knotted vector fields presented here encode a much larger variety of knots, possessing a richer structure, and studying their evolution could lead to new insights about the role of helicity in fluids [40] and plasmas [52,53], and novel topological solitons.

Finally, our systematic procedure for calculating the helicity of the knotted field $\mathbf{B}$ may help accurately determine the Hopf charge of arbitrarily knotted Skyrme-Faddeev solitons [27,29] and help tighten the lower bound on how their minimum energy grows with their Hopf charge [77].

The authors are grateful to Ben Bode for useful discussions and to the KITP and the Newton Institute for hospitality during the early part of this work. W. T. M. I. acknowledges support from the National Science Foundation (NSF) Grant No. DMR-1351506 and the Packard Foundation; D. F. and M. R. D. acknowledge support from the Leverhulme Trust, Research Programme Grant No. RP2013-K-009, "Scientific Properties of Complex Knots."

*hridesh@uchicago.edu

[1] H. K. Moffatt, J. Fluid Mech. **35**, 117 (1969).
[2] A. Enciso and D. Peralta-Salas, Ann. Math. **175**, 345 (2012).
[3] D. Kleckner and W. T. M. Irvine, Nat. Phys. **9**, 253 (2013).

[4] M. W. Scheeler, D. Kleckner, D. Proment, G. L. Kindlmann, and W. T. M. Irvine, Proc. Natl. Acad. Sci. U.S.A. **111**, 15350 (2014).
[5] C. F. Barenghi, Milan J. Math. **75**, 177 (2007).
[6] Y. Kawaguchi, M. Nitta, and M. Ueda, Phys. Rev. Lett. **100**, 180403 (2008).
[7] D. S. Hall, M. W. Ray, K. Tiurev, E. Ruokokoski, A. H. Gheorghe, and M. Möttönen, Nat. Phys. **12**, 478 (2016).
[8] D. Kleckner, L. H. Kauffman, and W. T. M. Irvine, Nat. Phys. **12**, 650 (2016).
[9] A. M. Kamchatnov, Sov. Phys. JETP **55**, 69 (1982).
[10] H. K. Moffatt, J. Fluid Mech. **159**, 359 (1985).
[11] A. F. Ranada, Lett. Math. Phys. **18**, 97 (1989).
[12] A. Y. K. Chui and H. K. Moffatt, Proc. R. Soc. A **451**, 609 (1995).
[13] W. T. M. Irvine and D. Bouwmeester, Nat. Phys. **4**, 716 (2008).
[14] W. T. M. Irvine, J. Phys. A **43**, 385203 (2010).
[15] M. Arrayas and J. L. Trueba, J. Phys. A **48**, 025203 (2015).
[16] A. Thompson, J. Swearngin, A. Wickes, and D. Bouwmeester, Phys. Rev. E **89**, 043104 (2014).
[17] C. B. Smiet, S. Candelaresi, A. Thompson, J. Swearngin, J. W. Dalhuisen, and D. Bouwmeester, Phys. Rev. Lett. **115**, 095001 (2015).
[18] A. F. Ranada, M. Soler, and J. L. Trueba, Phys. Rev. E **62**, 7181 (2000).
[19] H. Kedia, I. Bialynicki-Birula, D. Peralta-Salas, and W. T. M. Irvine, Phys. Rev. Lett. **111**, 150404 (2013).
[20] U. Tkalec, M. Ravnik, S. Copar, S. Zumer, and I. Musevic, Science **333**, 62 (2011).
[21] G. P. Alexander, B. G.-g. Chen, E. A. Matsumoto, and R. D. Kamien, Rev. Mod. Phys. **84**, 497 (2012).
[22] T. Machon and G. P. Alexander, Proc. Natl. Acad. Sci. U.S.A. **110**, 14174 (2013).
[23] A. Martinez, M. Ravnik, B. Lucero, R. Visvanathan, S. Zumer, and I. I. Smalyukh, Nat. Mater. **13**, 258 (2014).
[24] M. V. Berry and M. R. Dennis, Proc. R. Soc. A **456**, 2059 (2000).
[25] M. R. Dennis, R. P. King, B. Jack, K. O'Holleran, and M. J. Padgett, Nat. Phys. **6**, 118 (2010).
[26] L. Faddeev and A. J. Niemi, Nature (London) **387**, 58 (1997).
[27] R. A. Battye and P. M. Sutcliffe, Proc. R. Soc. A **455**, 4305 (1999).
[28] E. Babaev, L. D. Faddeev, and A. J. Niemi, Phys. Rev. B **65**, 100512 (2002).
[29] P. Sutcliffe, Proc. R. Soc. A **463**, 3001 (2007).
[30] A. J. Taylor and M. R. Dennis, Nat. Commun. **7**, 12346 (2016).
[31] E. Babaev, Phys. Rev. Lett. **88**, 177002 (2002).
[32] E. Babaev, Phys. Rev. B **79**, 104506 (2009).
[33] H. Helmholtz, J. Reine Angew. Math. **1858**, 25 (1858).
[34] W. Thomson, Proc. R. Soc. Edinburgh **6**, 94 (1869).
[35] L. Woltjer, Proc. Natl. Acad. Sci. U.S.A. **44**, 489 (1958).
[36] S. Chandrasekhar and L. Woltjer, Proc. Natl. Acad. Sci. U.S.A. **44**, 285 (1958).
[37] W. A. Newcomb, Ann. Phys. (N.Y.) **3**, 347 (1958).
[38] R. Monchaux, M. Berhanu, S. Aumatre, A. Chiffaudel, F. Daviaud, B. Dubrulle, F. Ravelet, S. Fauve, N. Mordant, F. Ptrlis, M. Bourgoin, P. Odier, J.-F. Pinton, N. Plihon, and R. Volk, Phys. Fluids **21**, 035108 (2009).
[39] M. Steenbeck, F. Krause, and K.-H. Rdler, Z. Naturforsch., A: Phys. Sci. **21**, 369 (2014).
[40] H. K. Moffatt, Proc. Natl. Acad. Sci. U.S.A. **111**, 3663 (2014).
[41] V. I. Arnold, *The asymptotic Hopf invariant and its applications* (Springer-Verlag, Berlin, 1974).
[42] M. H. Freedman, J. Fluid Mech. **194**, 549 (1988).
[43] H. K. Moffatt, J. Plasma Phys. **81**, 905810608 (2015).
[44] M. M. Rogers and P. Moin, Phys. Fluids **30**, 2662 (1987).
[45] J. M. Wallace, J.-L. Balint, and L. Ong, Phys. Fluids A: Fluid Dyn. **4**, 2013 (1992).
[46] H. K. Moffatt, Nature (London) **347**, 367 (1990).
[47] V. Katritch, J. Bednar, D. Michoud, R. G. Scharein, J. Dubochet, and A. Stasiak, Nature (London) **384**, 142 (1996).
[48] P. Pieranski and S. Przybyl, Phys. Rev. E **64**, 031801 (2001).
[49] R. V. Buniy and T. W. Kephart, Phys. Lett. B **576**, 127 (2003).
[50] R. V. Buniy and T. W. Kephart, Int. J. Mod. Phys. A **20**, 1252 (2005).
[51] R. V. Buniy, J. Cantarella, T. W. Kephart, and E. J. Rawdon, Phys. Rev. D **89**, 054513 (2014).
[52] H. K. Moffatt, Proc. R. Soc. A **472**, 20160183 (2016).
[53] S. R. Hudson, E. Startsev, and E. Feibush, Phys. Plasmas **21**, 010705 (2014).
[54] J. Milnor, *Singular Points of Complex Hypersurfaces* (Princeton University Press, Princeton, NJ, 1969).
[55] K. Brauner, Abh. Math. Semin. Univ. Hambg. **6**, 1 (1928).
[56] B. Perron, Inventiones Mathematicae **65**, 441 (1982).
[57] A. J. Taylor and M. R. Dennis, J. Phys. A **47**, 465101 (2014).
[58] D. W. Lyons, Math. Mag. **76**, 87 (2003).
[59] H. K. Urbantke, J. Geom. Phys. **46**, 125 (2003).
[60] R. Mosseri and J.-F. Sadoc, Structural chemistry **23**, 1071 (2012).
[61] J. F. Sadoc and J. Charvolin, J. Phys. A **42**, 465209 (2009).
[62] R. P. King, Ph. D. Thesis, University of Southampton, 2010.
[63] B. Bode, M. R. Dennis, D. Foster, and R. P. King, arXiv:1611.02563.
[64] P. Jennings, J. Phys. A **48**, 315401 (2015).
[65] See Supplemental Material at http://link.aps.org/supplemental/10.1103/PhysRevLett.117.274501 for more details on: progressing from the choice of a knot to a knotted field, smoothly restricting knotted fields to a knotted torus, and knotted fields with vanishing total helicity.
[66] Helicity in these flux tubes is gauge invariant [1,67] because $\mathbf{B} \cdot \mathbf{n} = 0$ on the surface of these flux tubes; i.e., they are magnetic surfaces.
[67] M. A. Berger and G. B. Field, J. Fluid Mech. **147**, 133 (1984).
[68] C. J. Houghton, N. S. Manton, and P. M. Sutcliffe, Nucl. Phys. **B510**, 507 (1998).
[69] D. Stern, J. Geophys. Res. **72**, 3995 (1967).
[70] D. P. Stern, Am. J. Phys. **38**, 494 (1970).
[71] M. Hesse and K. Schindler, J. Geophys. Res. **93**, 5559 (1988).
[72] K. K. Khurana, J. Geophys. Res. **102**, 11295 (1997).

[73] R. Rosner, B. C. Low, K. Tsinganos, and M. A. Berger, Geophys. Astrophys. Fluid Dyn. **48**, 251 (1989).
[74] J. H. C. Whitehead, Proc. Natl. Acad. Sci. U.S.A. **33**, 117 (1947).
[75] Mathematically, $\psi(u, v)$ takes its value on the complex projective plane, $\mathbb{CP}^1$ (i.e., the complex numbers with the point at ∞), which is homeomorphic to the 2-sphere S^2; in this sense, helicity can be understood as the topological degree of the map $S^3 \to S^2$.
[76] L. Rudolph, Commentarii mathematici Helvetici **62**, 630 (1987).
[77] R. S. Ward, Nonlinearity **12**, 241 (1999).